




Cite this: *RSC Adv.*, 2017, 7, 28723

A single fluorescent chemosensor for multiple targets of Cu²⁺, Fe^{2+/3+} and Al³⁺ in living cells and a near-perfect aqueous solution†

Tae Geun Jo,^a Jae Min Jung,^{*a} Jiyeon Han,^b Mi Hee Lim ^b and Cheal Kim ^{*a}

A sulfonate-based chemosensor **1** was designed and synthesized for sensing various analytes: Cu²⁺, Fe^{2+/3+} and Al³⁺. Sensor **1** showed a high selectivity and sensitivity for the analytes in a near-perfect aqueous medium. Cu²⁺ and Fe^{2+/3+} could be monitored by fluorescence quenching of **1**. It had sufficiently low detection limits (1.25 μM for Cu²⁺ and 3.96 μM for Fe³⁺), which were below the recommended levels of the World Health Organization for Cu²⁺ (31.5 μM) and the Environmental Protection Agency for Fe³⁺ (5.37 μM). **1** showed the high preferential selectivity for Cu²⁺ and Fe³⁺ in the presence of competitive metal ions without any interference. Importantly, pyrophosphate could be used to distinguish Fe³⁺ from Cu²⁺. In addition, this sensor could monitor Al³⁺ through fluorescence emission change. Moreover, **1** was successfully applied to quantify and image Al³⁺ in water samples and living cells. Based on photophysical studies and theoretical calculations, the sensing mechanisms of **1** for Cu²⁺ and Al³⁺ were explained, respectively.

Received 17th May 2017

Accepted 24th May 2017

DOI: 10.1039/c7ra05565j

rsc.li/rsc-advances

1. Introduction

Development of chemosensors with high selectivity and sensitivity for specific metal ions has been important due to their significant roles in medical, industrial, environmental and biological processes.¹ Among various metals, copper ions are the third abundant transition metal in the human body. They play diverse and significant roles in many biochemical processes in organisms from bacteria to mammals.^{2–7} However, a deficiency or overbalance of copper ions in human body can cause fatal diseases, such as Alzheimer's and Wilson's diseases.^{8–13}

As the first most abundant metal ions in human body, iron plays crucial roles in numerous biological processes, including electron transport function, synthesis of hemoglobin and immune system.^{14–18} On the contrary, disruption of iron-ion homeostasis can induce a number of severe neurological diseases with diverse clinical manifestations, ranging from anemia to iron overload.¹⁹ Aluminum is the third most abundant element on earth and extensively used in food additives, pharmaceutical synthesis, cosmetics and the manufacturing

industry.^{20–22} Due to its extensive use, aluminum can be easily accumulated in human body. Such accumulation of the metal ion could lead neuronal disorders such as Parkinson's disease and Alzheimer's disease.^{23–30} Therefore, the development of the chemosensors that could successfully recognize and determine these metal ions should be urgently developed.

In recent years, multiple target sensors for metal ions are attracting considerable interest, because they could abbreviate the processes to synthesize multiple compounds and facilitate to detect multiple analytes with a single device.^{3–7,11–13,16–18,20–22,31–36} However, there are still challenges to develop the sensors that could simultaneously detect and distinguish different target metal ions.

Sulfonic acid groups have been used to improve the solubility of chemosensors and naphthol moiety is a well-known excellent fluorophore.^{36–46} Therefore, we expected that the presence of a sulfonic acid group and a naphthol moiety in a chemosensor might not only increase its water solubility, but also have good optical properties.

Herein, we report the synthesis, characterization and fluorescent sensing behaviors of sulfonate-based sensor **1**, triethylammonium (*E*)-3-hydroxy-4-(((2-hydroxynaphthalen-1-yl)methylene)amino)naphthalene-1-sulfonate. Sensor **1** could recognize selectively Cu²⁺ and Fe^{2+/3+} by the fluorescence quenching and Al³⁺ by the obvious fluorescence emission change. Based on UV-vis and fluorescence titrations, Job plots, ESI-mass analyses, ¹H NMR titration and theoretical calculations, the sensing properties and mechanisms of **1** toward the three analytes were explained.

^aDepartment of Fine Chemistry, Department of Interdisciplinary Bio IT Materials, Seoul National University of Science and Technology, Seoul 139-743, Republic of Korea. E-mail: ianjemin@naver.com; chealkim@seoultech.ac.kr; Fax: +82-2-973-9149; Tel: +82-2-970-6693

^bDepartment of Chemistry, Ulsan National Institute of Science and Technology (UNIST), Ulsan 44919, Republic of Korea

† Electronic supplementary information (ESI) available: Experimental procedures and additional experimental data. See DOI: 10.1039/c7ra05565j



2. Experimental section

2.1. General information

All chemicals (analytical grade and spectroscopic grade) were purchased from Sigma-Aldrich and used without further purification. Both ^1H NMR and ^{13}C NMR were recorded on a Varian spectrometer (400 MHz for ^1H and 100 MHz for ^{13}C). The chemical shifts (δ) were recorded in ppm. Absorption spectra were recorded at room temperature using a Perkin Elmer model Lambda 2S UV/vis spectrophotometer. Fluorescence measurements were performed on a Perkin Elmer model LS45 fluorescence spectrophotometer. Electrospray ionization mass spectra (ESI-mass) were collected on a Thermo Finnigan (San Jose, CA, USA) LCQTM Advantage MAX quadrupole ion trap instrument. Elemental analysis for carbon, nitrogen and hydrogen was carried out by using a MICRO CUBE elemental analyzer (Germany) in Laboratory Center of Seoul National University of Science and Technology, Korea.

2.2. Synthesis of 1

4-Amino-3-hydroxynaphthalene-1-sulfonic acid (0.24 g, 1 mmol) and triethylammonium (TEA) were dissolved in 10 mL of methanol (MeOH). 2-Hydroxy-1-naphthaldehyde (0.17 g, 1 mmol) was added into the resulting solution. Then, the reaction solution was stirred for 5 h at room temperature. After evaporation, the product was recrystallized by diethyl ether and methanol, filtered and dried under vacuum. The yield: 0.17 g (34.4%). ^1H NMR (DMSO- d_6 , 400 MHz): δ 16.17 (s, 1H), 10.43 (s, 1H), 9.95 (d, $J = 3.6$ Hz, 1H), 8.83 (d, $J = 8.4$ Hz, 2H), 8.23 (d, $J = 8.4$ Hz, 1H), 7.99 (m, 3H), 7.86 (d, $J = 8.4$ Hz, 1H), 7.55 (q, $J = 8.0$ Hz, 2H), 7.39 (m, 2H), 7.13 (d, $J = 9.2$ Hz, 2H), 3.10 (m, 6H for TEA), 1.17 (t, $J = 7.2$, 9H for TEA). ^{13}C NMR (DMSO- d_6 , 100 MHz): δ 155.46, 155.35, 154.17, 146.13, 129.14, 113.15, 106.55, 105.85, 49.77, 49.29, 26.92, 21.86, 21.04, 20.60 ppm. ESI-mass: m/z calcd for $\text{C}_{21}\text{H}_{15}\text{NO}_5\text{S} - \text{H}^+$ ($[\text{M} - \text{H}^+]$), 392.06; found, 392.30.

2.3. Fluorescent sensing for Cu^{2+} , $\text{Fe}^{2+/3+}$ and Al^{3+}

Fluorescence titration measurements. For Cu^{2+} , $\text{Cu}(\text{NO}_3)_2$ stock solution (9 mM) was prepared in Bis-Tris buffer solution. 2.5–25 μL of the Cu^{2+} solution were diluted to Bis-Tris buffer solution. Each vial had a total volume of 2.991 mL. Then, 9 μL of sensor 1 solution (10 mM) was diluted to the prepared solution, separately. After stirring them for a few seconds, fluorescence spectra were recorded at room temperature. The same procedure was also applied to $\text{Fe}^{2+/3+}$ and Al^{3+} .

Job plot measurements. 90 μL of sensor 1 solution (10 mM) was diluted to 29.91 mL of Bis-Tris buffer solution to make the concentration of 30 μM . 90 μL of Cu^{2+} solution (10 mM) was diluted to 29.91 mL of Bis-Tris buffer solution. 2.7, 2.4, 2.1, 1.8, 1.5, 1.2, 0.9, 0.6 and 0.3 mL of the Cu^{2+} solution were taken and transferred to vials. 0.3, 0.6, 0.9, 1.2, 1.5, 1.8, 2.1, 2.4 and 2.7 mL of the 1 solution were added to each Cu^{2+} solution separately. Each vial had a total volume of 3 mL. After stirring them for a few seconds, fluorescence spectra were recorded at room

temperature. The same procedure was also applied to $\text{Fe}^{2+/3+}$ and Al^{3+} .

Competition tests. Stock solutions of MNO_3 ($\text{M} = \text{Na}, \text{K}$) or $\text{M}(\text{NO}_3)_2$ ($\text{M} = \text{Zn}, \text{Cd}, \text{Cu}, \text{Mg}, \text{Co}, \text{Ni}, \text{Ca}, \text{Mn}, \text{Pb}$) or $\text{M}(\text{NO}_3)_3$ ($\text{M} = \text{Al}, \text{Ga}, \text{In}, \text{Fe}, \text{Cr}$) or $\text{M}(\text{ClO}_4)_2$ ($\text{M} = \text{Fe}$) were prepared in Bis-Tris buffer solution, respectively.

For Cu^{2+} , 20 μL of each metal-ion solution (9 mM) was diluted to Bis-Tris buffer solution, respectively. 20 μL of Cu^{2+} solution (9 mM) was added to the solutions prepared above. Then, 9 μL of sensor 1 solution (10 mM) was added to the mixed solutions. Each vial had a total volume of 3 mL. After stirring them for a few seconds, fluorescence spectra were recorded at room temperature.

For Fe^{3+} , 40 μL of each metal-ion solution (9 mM) was diluted to Bis-Tris buffer solution, respectively. 40 μL of Fe^{3+} solution (9 mM) was added to the solutions prepared above. Then, 9 μL of sensor 1 solution (10 mM) was added to the mixed solutions. Each vial had a total volume of 3 mL. After stirring them for a few seconds, fluorescence spectra were recorded at room temperature.

For Al^{3+} , 67.5 μL of each metal-ion solution (100 mM) was diluted to Bis-Tris buffer solution, respectively. 67.5 μL of Al^{3+} solution (100 mM) was added to the solutions prepared above. Then, 9 μL of sensor 1 solution (10 mM) was added to the mixed solutions. Each vial had a total volume of 3 mL. After stirring them for a few seconds, fluorescence spectra were recorded at room temperature.

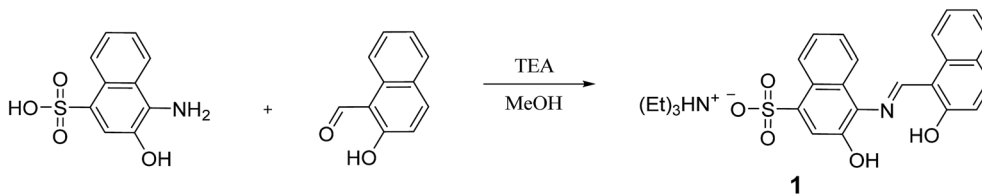
^1H NMR titrations. For ^1H NMR titrations of sensor 1 with Al^{3+} , three NMR tubes of sensor 1 (0.01 mmol) dissolved in DMSO- d_6 were prepared and then three different concentrations (0, 0.005 and 0.01 mmol) of $\text{Al}(\text{NO}_3)_3$ dissolved in DMF- d_7 were added to each sensor 1 solution. After stirring them for a few seconds, ^1H NMR spectra were recorded at room temperature.

Imaging experiments in living cells. HeLa cells (ATCC, Manassas, USA) were maintained in media containing DMEM, 10% fetal bovine serum (FBS, GIBCO, Grand Island, NY, USA), 100 U mL^{-1} penicillin (GIBCO), and 100 mg mL^{-1} streptomycin (GIBCO). The cells grew in a humidified atmosphere with 5% CO_2 at 37 $^\circ\text{C}$. Cells were seeded onto 6 well plate (SPL Life Sciences Co., Ltd., South Korea) at a density of 150 000 cells per 1 mL and then incubated at 37 $^\circ\text{C}$ for 12 h. For fluorescence imaging experiments, cells were first treated with 1 (dissolved in DMSO; 1% v/v final DMSO concentration; 20 μM ; at room temperature) for 10 min. After incubation with aluminum nitrite (dissolved in water; 1% v/v DMSO; 200 μM) for 10 min, cells were washed with 2 mL of 10 mM Bis-Tris buffer (pH 7.4, 150 mM NaCl) two times. Imaging was performed with an EVOS FL fluorescence microscope (Life technologies) using a GFP light cube [excitation 470 (± 11) nm; emission 510 (± 21) nm].

2.4. Theoretical calculations

All theoretical calculations based on the hybrid exchange correlation functional B3LYP^{47,48} applying the 6-31G** basis set^{49,50} was employed for the main group elements, whereas the LanL2DZ effective core potential (ECP)^{51,52} was used for Cu. In





Scheme 1 Synthetic procedure of 1.

vibrational frequency calculations, there was no imaginary frequency for the optimized geometries of **1**, **1**-Al³⁺ and **1**-Cu²⁺ complex, suggesting that these geometries represented local minima. In order to investigate the transition energies for the optimized structures of **1**, **1**-Al³⁺ and **1**-Cu²⁺ species, twenty lowest singlets were calculated with TD-DFT (B3LYP). The GaussSum 2.1 (ref. 53) was used to calculate the contributions of molecular orbitals in electronic transitions. All the calculations were carried out using Gaussian 03 program.⁵⁴

3. Results and discussion

Chemosensor **1** was synthesized by the condensation reaction of 4-amino-3-hydroxynaphthalene-1-sulfonic acid with 2-hydroxy-1-naphthaldehyde in methanol (Scheme 1), and characterized by ¹H (Fig. S1†) and ¹³C NMR, ESI-mass spectrometry and elemental analysis.

The fluorescence sensing ability of **1** was examined toward various metal ions such as Al³⁺, Ga³⁺, In³⁺, Zn²⁺, Cd²⁺, Cu²⁺, Fe²⁺, Fe³⁺, Mg²⁺, Cr³⁺, Co²⁺, Ni²⁺, Na⁺, K⁺, Ca²⁺, Mn²⁺ and Pb²⁺ in Bis-Tris buffer solution (10 mM, pH 7.0) (Fig. 1). Upon excitation at 380 nm, **1** exhibited a fluorescence emission at 442 nm. In the presence of most cations, there was no significant change in the fluorescence spectrum, whereas Cu²⁺, Fe²⁺, Fe³⁺ and Al³⁺ ions showed the notable spectral changes. In cases of Cu²⁺, Fe²⁺ and Fe³⁺, the emission intensity of **1** at 442 nm was completely quenched. Meanwhile, the fluorescence emission at 442 nm was red-shifted to 535 nm in the presence of Al³⁺. Therefore, **1** might be a potential fluorescence chemosensor that could detect copper and iron ions by fluorescence quenching and aluminum ion by fluorescence emission change.

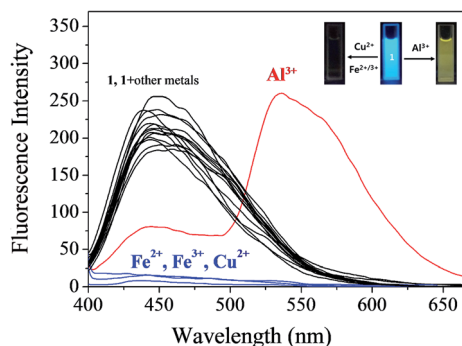


Fig. 1 Fluorescence spectral change of **1** (30 μM) upon addition of 70 equiv. of different metal ions in Bis-Tris buffer (10 mM Bis-Tris, pH 7.0).

3.1. Turn-off fluorescence detection of Cu²⁺ and Fe^{2+/3+}

The fluorescence and UV-vis titration experiments were conducted to understand the binding property of **1** with Cu²⁺. Upon the addition of Cu²⁺, the fluorescence emission intensity of **1** at 442 nm steadily decreased and quenched until amount of Cu²⁺ reached 2 equiv. (Fig. 2). The UV-vis titration showed that the absorption bands of **1** at 320 nm and 450 nm decreased, while the bands at 270 nm and 467 nm increased gradually (Fig. S2†). Two isosbestic points at 302 nm and 458 nm indicated the formation of the only one species between **1** and Cu²⁺.

In order to examine the binding stoichiometry of **1** with Cu²⁺, Job plot analysis was carried out (Fig. S3†). A maximum intensity appeared at the molar fraction of 0.5, which indicated a 1 : 1 binding mode between **1** and Cu²⁺. To further confirm the binding mode between **1** and Cu²⁺, ESI-mass spectrometry analysis was conducted (Fig. 3). The negative mass data of **1** for

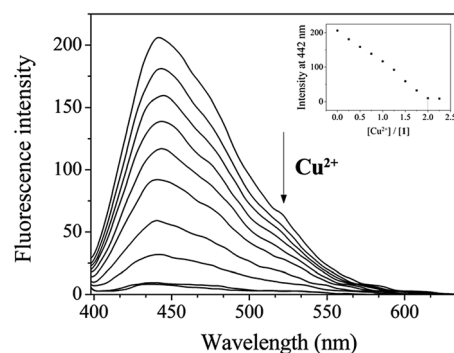


Fig. 2 Fluorescence spectral change of **1** (30 μM) with Cu²⁺ ions (0–2.25 equiv.) in Bis-Tris buffer (10 mM, pH 7.0).

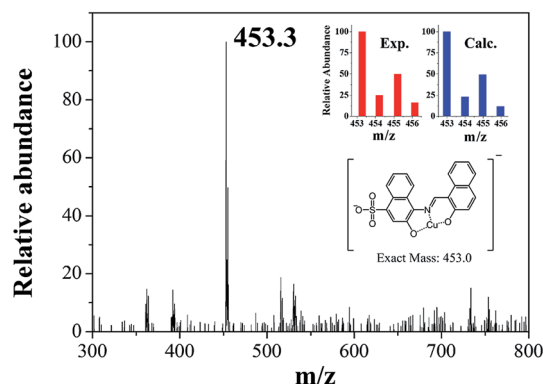


Fig. 3 Negative-ion ESI-mass spectrum of **1** (100 μM) upon addition of 1 equiv. of Cu²⁺.



Cu^{2+} showed that the peak at $m/z = 453.3$ was assignable to $1-3\text{H}^+ + \text{Cu}^{2+}$ [calcd, m/z : 453.0]. Based on the titration measurement, the association constant (K) of **1** with Cu^{2+} was calculated as $4.8 \times 10^3 \text{ M}^{-1}$ by Benesi-Hildebrand equation⁵⁵ (Fig. S4†), which was within the range of those (10^3 to 10^{12}) previously reported for chemosensors toward Cu^{2+} .⁵⁶⁻⁶¹ As shown in Fig. S5,† the detection limit ($3\sigma/k$)⁶² of **1** for Cu^{2+} was determined to be $1.25 \mu\text{M}$ which was much lower than that ($31.5 \mu\text{M}$) recommended by WHO in drinking water.⁶³

A preferential selectivity of **1** toward Cu^{2+} was evaluated in the presence of other competitive species (Al^{3+} , Ga^{3+} , In^{3+} , Zn^{2+} , Cd^{2+} , Fe^{2+} , Fe^{3+} , Mg^{2+} , Cr^{3+} , Co^{2+} , Ni^{2+} , Na^+ , K^+ , Ca^{2+} , Mn^{2+} and Pb^{2+}) (Fig. 4). There was no significant interference for sensing of Cu^{2+} . For practical application, the pH effects of **1** in the absence and presence of Cu^{2+} were investigated at various pH range of 2 to 12. The fluorescence quenching of **1** by adding Cu^{2+} was observed between pH 6 and 10 (Fig. S6†), which warrants its application for detection of Cu^{2+} under physiological pH 7.0–8.4.⁶⁴

Next, fluorescence titration of **1** toward Fe^{3+} was carried out to understand binding properties. Upon the addition of Fe^{3+} , the fluorescence intensity at 442 nm was gradually reduced and completely quenched when 4 equiv. of Fe^{3+} were added (Fig. 5). UV-vis titration of **1** for Fe^{3+} showed that the absorption at 450 nm decreased and those at 300 and 580 nm increased with two clear isosbestic points at 405 and 527 nm (Fig. S7†). The peak at 580 nm, which has a high molar extinction coefficient ($1.9 \times 10^3 \text{ M}^{-1} \text{ cm}^{-1}$), are too large to be Fe-based d-d transitions. Thus, the new peak might be due to a metal-to-ligand charge-transfer (MLCT).⁶⁵

Job plot analysis revealed a 1 : 1 stoichiometry for **1** and Fe^{3+} (Fig. S8†), which further was confirmed by ESI-mass spectrometry analysis. As shown in Fig. 6, the negative mass data of **1** for Fe^{3+} showed the major peak at $m/z = 508.0$, which was assigned to $1-3\text{H}^+ + \text{Fe}^{3+} + \text{NO}_3^-$ [calcd, m/z : 508.0]. The association constant (K) for Fe^{3+} was determined to be $1.1 \times 10^4 \text{ M}^{-1}$ by using Benesi-Hildebrand equation⁵⁵ (Fig. S9†), which was within the range of those (10^3 to 10^5) previously reported for chemosensors toward Fe^{3+} .⁶⁶ The detection limit ($3\sigma/k$)⁶² of **1** for Fe^{3+} was calculated to be $3.96 \mu\text{M}$ (Fig. S10†), which was lower than the guideline ($5.37 \mu\text{M}$) recommended by environmental protection agency guideline (EPA) for iron in drinking water.⁶³

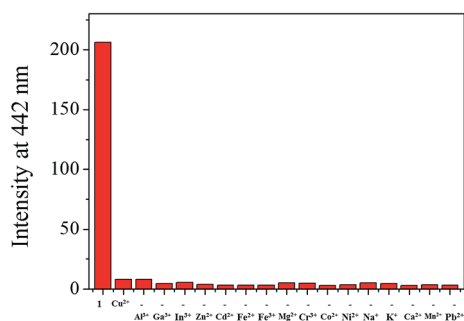


Fig. 4 Fluorescence intensity (at 442 nm) of **1** upon addition of Cu^{2+} ions (2.0 equiv.) in the absence and presence of other metal ions (2.0 equiv.).

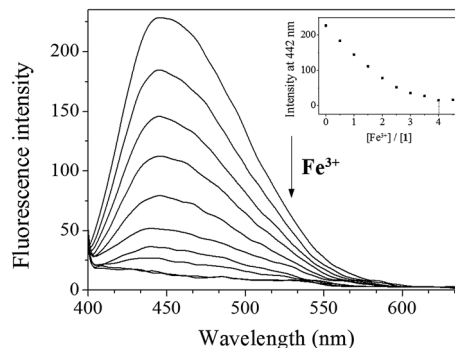


Fig. 5 Fluorescence spectral change of **1** ($30 \mu\text{M}$) with Fe^{3+} ions (0–4.5 equiv.) in Bis-Tris buffer (10 mM, pH 7.0).

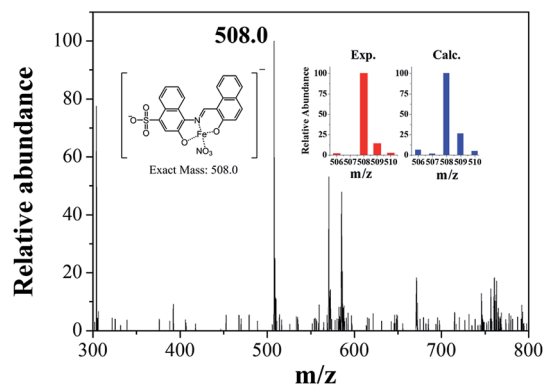


Fig. 6 Negative-ion ESI-mass spectrum of **1** ($100 \mu\text{M}$) upon addition of 1 equiv. of Fe^{3+} .

To examine the preferential selectivity for Fe^{3+} , the interference experiments were evaluated in the presence of other competitive species (Fig. 7). Compared with the fluorescence intensity of $1-\text{Fe}^{3+}$, there was no distinct variation in the presence of other metal ions. These results suggested that sensing properties of **1** for Fe^{3+} was hardly affected from potentially competitive metal ions. The pH sensitivity of Fe^{3+} detection by **1** was examined at various pH range of 2 to 12 (Fig. S11†). The fluorescence quenching of the $1-\text{Fe}^{3+}$ complex was exhibited between pH 2 and 10, which warrants that Fe^{3+} could be clearly detected by

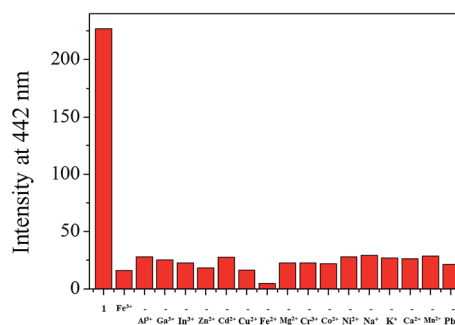


Fig. 7 Fluorescence intensity (at 442 nm) of **1** upon addition of Fe^{3+} ions (4.0 equiv.) in the absence and presence of other metal ions (4.0 equiv.).



fluorescence measurements using chemosensor **1** over a wide range of pH.

On the other hand, we also conducted the UV-vis titration of **1** for Fe²⁺ (Fig. S12†). The titration for Fe²⁺ was nearly identical to that of Fe³⁺. These results could be explained by the rapid oxidation reaction of Fe²⁺ to Fe³⁺ in the 1-Fe²⁺ complex by oxygen molecule.²⁸ To further verify our proposal, the UV-vis spectral changes of **1** for Fe²⁺ were observed under the degassed conditions (Fig. S13†). Upon the addition of Fe²⁺ into a solution of **1** under an anaerobic condition, there was no significant change in spectrum of **1**. Upon the exposure of 1-Fe²⁺ complex to air, however, the spectrum of 1-Fe²⁺ complex was dramatically changed, which was nearly identical to that of 1-Fe³⁺ complex. These observations indicated that 1-Fe²⁺ complex formed under the degassed conditions might be rapidly oxidized to 1-Fe³⁺ complex in air.

Some metal complexes showed the selectivity toward specific anions in the systems such as Cu-S, Cu-CN, and Hg-I.⁶⁷ Therefore, we also examined the selectivity of 1-Fe³⁺ and 1-Cu²⁺ complexes toward various anions, such as PPI (pyrophosphate), AMP, ADP, ATP, CN⁻, AcO⁻, F⁻, Cl⁻, Br⁻, I⁻, BzO⁻, N₃⁻, SCN⁻, H₂PO₄⁻, S²⁻, NO₃⁻ and SO₄²⁻ (Fig. S14†). Only PPI induced a recovery of fluorescence intensity toward 1-Fe³⁺ complex, while there was no change in fluorescence intensities of 1-Fe³⁺ and 1-Cu²⁺ complex solutions. It is worthwhile to mention that the fluorescence recovery of 1-Fe³⁺ complex by PPI is very useful, because it could distinguish 1-Fe³⁺ from 1-Cu²⁺ complex. As shown in Fig. 1, both 1-Fe³⁺ and 1-Cu²⁺ complexes exhibited the fluorescence quenching. If sensor **1** with the strong fluorescence intensity would show fluorescence quenching upon the addition of a certain metal

ion, it can be Cu²⁺ or Fe ion. In such a case, the fluorescence recovery of **1** by PPI would indicate that the metal ion could be Fe ion, while in the absence of the fluorescence recovery of **1** it could be Cu²⁺.

3.2. Detection of Al³⁺ by fluorescence emission change

To investigate the sensing properties of **1** toward Al³⁺, UV-vis and fluorescence titrations were performed in a near-perfect aqueous solution. On the gradual addition of Al³⁺, the fluorescence intensity at 442 nm decreased and a new emission band at 535 nm appeared (Fig. 8). The UV-titration experiments showed that the absorbance band at 425 nm decreased gradually, while the absorbance at 280 nm and 467 nm increased upon the gradual addition of Al³⁺ (Fig. S15†). The isosbestic points at 301 nm and 448 nm were observed, indicating that the binding between **1** and Al³⁺ ions afforded only one species.

The Job plot analysis⁶⁸ for **1** and Al³⁺ showed a 1 : 1 complexation (Fig. S16†). The binding mode of **1** and Al³⁺ was further confirmed by ESI-mass spectrometry analysis (Fig. S17†). The negative mass spectrum of **1** for Al³⁺ showed that the major peaks at *m/z* = 479.3 and 556.5 were assignable to 1-3H⁺ + Al³⁺ + NO₃⁻ [calcd, *m/z*: 479.0] and 1-3H⁺ + Al³⁺ + NO₃⁻ + DMSO [calcd, *m/z*: 557.0], respectively. Based on the fluorescence titration, the association constant (*K*) of **1** for Al³⁺ derived from Benesi-Hildebrand equation⁵⁵ was calculated to be 8.9 × 10⁴ M⁻¹ (Fig. S18†), which was within the range of those (10² to 10⁹) previously reported for Al³⁺-binding chemosensors.⁶⁹ The detection limit (3σ/*k*)⁶² of **1** as a fluorescence sensor for Al³⁺ sensing was determined to be 18.07 μM (Fig. S19†).

In order to confirm the selectivity of **1** for Al³⁺ over competing metal ions, the interference experiments were carried out (Fig. S20†). In the presence of Cu²⁺, Fe²⁺, Fe³⁺ and Cr³⁺, the relative emission intensity was inhibited, whereas most of other metal ions did not interfere with the detection of Al³⁺. The practical application of **1** was evaluated through pH dependent study. As shown in Fig. S21,† **1** could clearly detect Al³⁺ over a wide range of pH 4.0–11.0. To further check the practical applicability of sensor **1**, we conducted the real sample analysis for quantitative measurement of Al³⁺. A good calibration curve was constructed for the determination of Al³⁺ (Fig. S22†). Then, it was applied to determinate Al³⁺ ions in both artificial polluted and drinking water samples. As shown in Table 1, suitable recoveries and Relative Standard Deviation (R.S.D.) values of the water samples were obtained.

To investigate the sensing mechanism of **1** toward Al³⁺, ¹H NMR titration of **1** with Al³⁺ was carried out (Fig. 9). Upon the

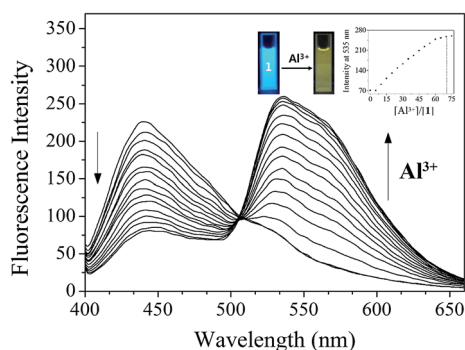


Fig. 8 Fluorescence spectral change of **1** (30 μM) with Al³⁺ ions (0–80 equiv.) in Bis-Tris buffer (10 mM, pH 7.0).

Table 1 Determination of Al³⁺ in water samples^a

Sample	Al(III) added (μmol L ⁻¹)	Al(III) found (μmol L ⁻¹)	Recovery (%)	R.S.D. (<i>n</i> = 3) (%)
Artificial polluted water ^b	300.0	303.8	101.3	1.40
Drinking water	300.0	296.9	99.0	0.96

^a Condition: [**1**] = 30 μmol L⁻¹ in Bis-Tris buffer (10 mM, pH 7.0). ^b Prepared by deionized water, 300 μmol L⁻¹: Zn²⁺, Cd²⁺, Pb²⁺, Hg²⁺, Na⁺, K⁺, Ca²⁺, Mg²⁺.



addition of Al^{3+} , the protons H_1 and H_2 disappeared, and the protons H_3 , H_5 and H_8 shifted slightly up-field. When more than 1 equiv. of Al^{3+} were added, there was no shift in the position of proton signals, which implied the 1 : 1 complexation of **1** with Al^{3+} .

To examine the potential of **1** to monitor Al^{3+} in living cells, fluorescence imaging experiments were conducted (Fig. 10). HeLa cells were first incubated with **1** for 10 min and then exposed to aqueous Al^{3+} solution for 10 min before imaging. The results showed that the HeLa cells without either Al^{3+} or **1** showed negligible intracellular fluorescence, while those cultured with both Al^{3+} and **1** exhibited fluorescence.

3.3. Theoretical calculations

Theoretical calculations were carried out to get deep insight into fluorescence sensing mechanisms of **1** toward Cu^{2+} and Al^{3+} in parallel to the experimental studies. Based on Job plots and ESI-mass spectrometry analyses, all theoretical calculations were considered with the 1 : 1 stoichiometry for the **1**- Cu^{2+} and **1**- Al^{3+} complexes. Moreover, for the simplicity of the calculations, the triethylammonium salt of **1** was replaced by a hydrogen atom (Fig. 11). The energy-minimized structures for **1**, **1**- Cu^{2+} and **1**- Al^{3+} complex were calculated by utilizing the density functional theory (DFT/B3LYP/main group atom and Al: 6-31G** and Cu: Lanl2DZ/ECP) (Fig. 11). The energy-minimized

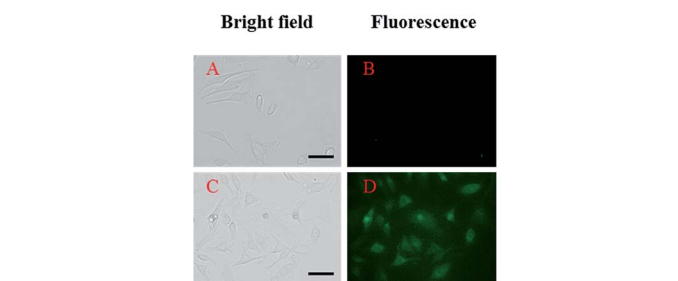


Fig. 10 Fluorescent responses of **1** to Al^{3+} in HeLa cells. Cells (A and B) were preincubated with **1** for 10 min prior to addition of Al^{3+} (C and D). The left side images (A and C) were observed with the light microscope and the right side images (B and D) were taken with a fluorescence microscope. Conditions: [**1**] = 20 μM ; [Al^{3+}] = 200 μM ; 37 $^\circ\text{C}$; 5% CO_2 .

structure (**1C**, **2C**, **3N**, **4C** = 128.9 $^\circ$) of **1** showed a twisted shape (Fig. 11a). After combined with Cu^{2+} or Al^{3+} , the structures of the complexes **1**- Cu^{2+} and **1**- Al^{3+} were flatter than that of **1** (**1C**, **2C**, **3N**, **4C** = 157.0 $^\circ$ for Cu^{2+} and **1C**, **2C**, **3N**, **4C** = 162.6 $^\circ$ for Al^{3+}) (Fig. 11b and c). Both Cu^{2+} and Al^{3+} were coordinated to the N atom in the Schiff-base and the two O atoms in the hydroxyl groups of **1**.

We further investigated the singlet excited states of **1**, **1**- Cu^{2+} and **1**- Al^{3+} species by using the TD-DFT (time dependent-density functional theory) methods, which were compared with their UV-vis spectra. In case of **1**, the main molecular

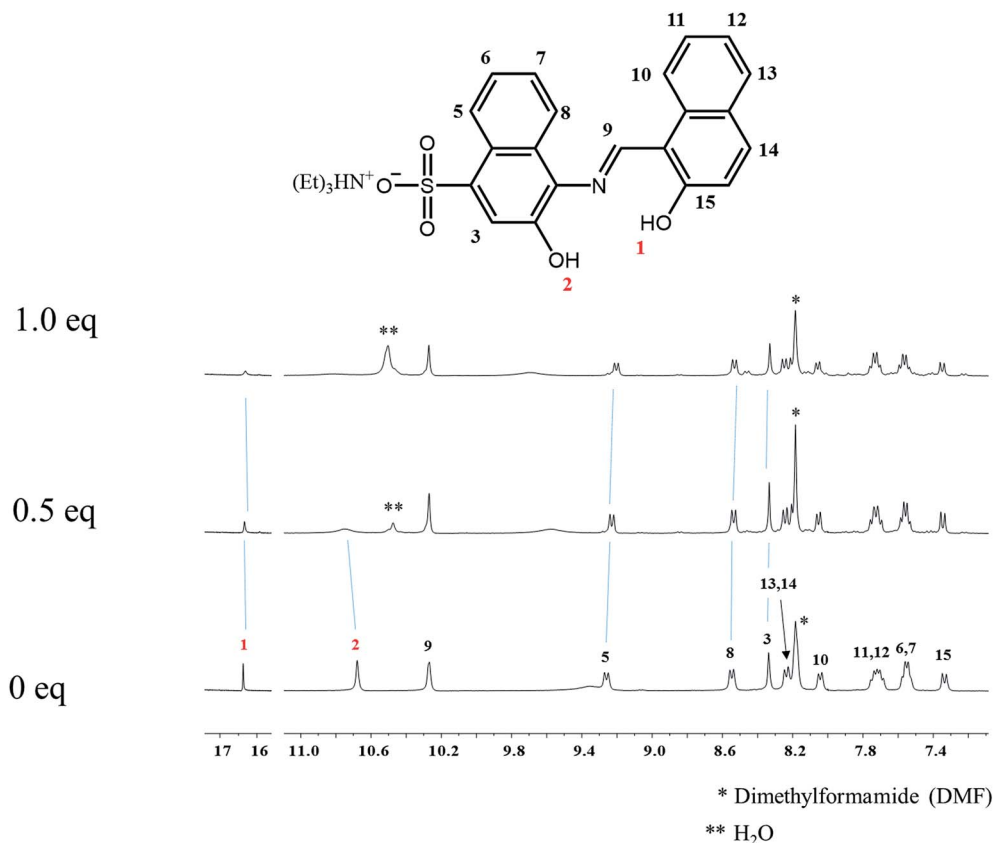


Fig. 9 ^1H NMR titrations of **1** with Al^{3+} (0, 0.5 and 1.0 equiv.).



- 13 X. Xue, H. Fang, H. Chen, C. Zhang, C. Zhu, Y. Bai, W. He and Z. Guo, *Dyes Pigm.*, 2016, **130**, 116–121.
- 14 D. Duy, G. Wanner, A. R. Meda, N. von Wirén, J. Soll and K. Philipp, *Plant Cell*, 2007, **19**, 986–1006.
- 15 M. W. Hentze, M. U. Muckenthaler and N. C. Andrews, *Cell*, 2004, **117**, 285–297.
- 16 K. B. Kim, H. Kim, E. J. Song, S. Kim, I. S. Noh and C. Kim, *Dalton Trans.*, 2013, **42**, 16569–16577.
- 17 F. Ge, H. Ye, H. Zhang and B.-X. Zhao, *Dyes Pigm.*, 2013, **99**, 661–665.
- 18 Z. Li, Y. Zhou, K. Yin, Z. Yu, Y. Li and J. Ren, *Dyes Pigm.*, 2014, **105**, 7–11.
- 19 P. T. Lieu, M. Heiskala, P. A. Peterson and Y. Yang, *Mol. Aspects Med.*, 2001, **22**, 1–87.
- 20 D. Maity and T. Govindaraju, *Inorg. Chem.*, 2010, **49**, 7229–7231.
- 21 D. Maity and T. Govindaraju, *Eur. J. Inorg. Chem.*, 2011, **2011**, 5479–5485.
- 22 S. Pu, C. Zhang, C. Fan and G. Liu, *Dyes Pigm.*, 2016, **129**, 24–33.
- 23 B. R. Stephens and J. S. Jolliff, *Diet and Nutrition in Dementia and Cognitive Decline*, 2014, pp. 553–562.
- 24 P. Nayak, *Environ. Res.*, 2002, **89**, 101–115.
- 25 D. Sarkar, P. Ghosh, S. Gharami, T. K. Mondal and N. Murmu, *Sens. Actuators, B*, 2017, **242**, 338–346.
- 26 S. Y. Li, D. B. Zhang, J. Y. Wang, R. M. Lu, C. H. Zheng and S. Z. Pu, *Sens. Actuators, B*, 2017, **245**, 263–267.
- 27 J. Jun Lee, G. Jin Park, Y. Sung Kim, S. Young Lee, H. Ji Lee, I. S. Noh and C. Kim, *Biosens. Bioelectron.*, 2015, **69**, 226–229.
- 28 Y. W. Choi, G. J. Park, Y. J. Na, H. Y. Jo, S. A. Lee, G. R. You and C. Kim, *Sens. Actuators, B*, 2014, **194**, 343–352.
- 29 S. A. Lee, G. R. You, Y. W. Choi, H. Y. Jo, A. R. Kim, I. Noh, S.-J. Kim, Y. Kim, C. Kim, X. Bu and D. Das, *Dalton Trans.*, 2014, **43**, 6650–6659.
- 30 Y. K. Jang, U. C. Nam, H. L. Kwon, I. H. Hwang and C. Kim, *Dyes Pigm.*, 2013, **99**, 6–13.
- 31 E. J. Song, J. Kang, G. R. You, G. J. Park, Y. Kim, S.-J. Kim, C. Kim and R. G. Harrison, *Dalton Trans.*, 2013, **42**, 15514–15520.
- 32 H. J. Jung, N. Singh, D. Y. Lee and D. O. Jang, *Tetrahedron Lett.*, 2010, **51**, 3962–3965.
- 33 H. Yang, H. Song, Y. Zhu and S. Yang, *Tetrahedron Lett.*, 2012, **53**, 2026–2029.
- 34 V. K. Gupta, A. K. Singh and B. Gupta, *Anal. Chim. Acta*, 2006, **575**, 198–204.
- 35 H. A. Tajmir-Riahi, *Polyhedron*, 1983, **2**, 723–726.
- 36 B.-L. Wang, C. Jiang, K. Li, Y.-H. Liu, Y. Xie and X.-Q. Yu, *Analyst*, 2015, **140**, 4608–4615.
- 37 A. Atahan and S. Durmus, *Spectrochim. Acta, Part A*, 2015, **144**, 61–67.
- 38 B. Shi, P. Zhang, T. Wei, H. Yao, Q. Lin and Y. Zhang, *Chem. Commun.*, 2013, **49**, 7812–7814.
- 39 A. Syamal and M. M. Singh, *React. Polym.*, 1993, **21**, 149–158.
- 40 F. Y. Wu, H. Zhang, M. Xiao and B. X. Han, *Spectrochim. Acta, Part A*, 2013, **109**, 221–225.
- 41 S. Goswami, A. Manna, S. Paul, C. Kheng Quah and H.-K. Fun, *Chem. Commun.*, 2013, **49**, 11656–11658.
- 42 V. K. Gupta, A. K. Singh and L. K. Kumawat, *Sens. Actuators, B*, 2014, **195**, 98–108.
- 43 K. Tiwari, M. Mishra, V. P. Singh, S. Lohar, D. Karak, B. Sarkar, S. K. Mukhopadhyay, A. K. Mukherjee, D. Das and L. Tian, *RSC Adv.*, 2013, **3**, 12124–12132.
- 44 Z. Liu, Y. Li, Y. Ding, Z. Yang, B. Wang, Y. Li, T. Li, W. Luo, W. Zhu, J. Xie and C. Wang, *Sens. Actuators, B*, 2014, **197**, 200–205.
- 45 B. Liu, P. Wang, J. Chai, X. Hu, T. Gao, J. Chao, T. Chen and B. Yang, *Spectrochim. Acta, Part A*, 2016, **168**, 98–103.
- 46 H.-Y. Lin, T.-Y. Chen, C.-K. Liu and A.-T. Wu, *Luminescence*, 2016, **31**, 236–240.
- 47 A. D. Becke, *J. Chem. Phys.*, 1993, **98**, 5648.
- 48 C. Lee, W. Yang and R. G. Parr, *Phys. Rev. B: Condens. Matter Mater. Phys.*, 1988, **37**, 785–789.
- 49 P. C. Hariharan and J. A. Pople, *Theor. Chim. Acta*, 1973, **28**, 213–222.
- 50 M. M. Francl, W. J. Pietro, W. J. Hehre, J. S. Binkley, M. S. Gordon, D. J. DeFrees and J. A. Pople, *J. Chem. Phys.*, 1982, **77**, 3654–3665.
- 51 W. R. Wadt and P. J. Hay, *J. Chem. Phys.*, 1985, **82**, 284–298.
- 52 P. J. Hay and W. R. Wadt, *J. Chem. Phys.*, 1985, **82**, 270.
- 53 N. M. O'boyle, A. L. Tenderholt and K. M. Langner, *J. Comput. Chem.*, 2008, **29**, 839–845.
- 54 R. M. Yucel, Y. He and A. M. Zaslavsky, *Stat. Med.*, 2011, **30**, 3447–3460.
- 55 H. A. Benesi and J. H. Hildebrand, *J. Am. Chem. Soc.*, 1949, **71**, 2703–2707.
- 56 Y. Hu, J. Zhang, Y.-Z. Lv, X.-H. Huang and S. Hu, *Spectrochim. Acta, Part A*, 2016, **157**, 164–169.
- 57 S. Samanta, U. Manna, T. Ray and G. Das, *Dalton Trans.*, 2015, **44**, 18902–18910.
- 58 G. R. You, G. J. Park, J. J. Lee and C. Kim, *Dalton Trans.*, 2015, **44**, 9120–9129.
- 59 T. G. Jo, Y. J. Na, J. J. Lee, M. M. Lee, S. Y. Lee and C. Kim, *Sens. Actuators, B*, 2015, **211**, 498–506.
- 60 L. Tang, J. Zhao, M. Cai, P. Zhou, K. Zhong, S. Hou and Y. Bian, *Tetrahedron Lett.*, 2013, **54**, 6105–6109.
- 61 S. Goswami, S. Maity, A. K. Das and A. C. Maity, *Tetrahedron Lett.*, 2013, **54**, 6631–6634.
- 62 Y. K. Tsui, S. Devaraj and Y. P. Yen, *Sens. Actuators, B*, 2012, **161**, 510–519.
- 63 N. Graham, *Urban Water*, 1999, **1**, 183.
- 64 R. M. Harrison, D. P. H. Laxen and S. J. Wilson, *Environ. Sci. Technol.*, 1981, **15**, 1378–1383.
- 65 M. A. R. Meier and U. S. Schubert, *Chem. Commun.*, 2005, 4610–4612.
- 66 G. R. You, G. J. Park, S. A. Lee, K. Y. Ryu and C. Kim, *Sens. Actuators, B*, 2015, **215**, 188–195.
- 67 G. J. Park, Y. J. Na, H. Y. Jo, S. A. Lee and C. Kim, *Dalton Trans.*, 2014, **43**, 6618–6622.
- 68 P. Job, *Ann. Chim.*, 1928, **9**, 113–203.



- 69 L. Wang, H. Li and D. Cao, *Sens. Actuators, B*, 2013, **181**, 749–755.
- 70 H. S. Jung, P. S. Kwon, J. W. Lee, J. Il Kim, C. S. Hong, J. W. Kim, S. Yan, J. Y. Lee, J. H. Lee, T. Joo and J. S. Kim, *J. Am. Chem. Soc.*, 2009, **131**, 2008–2012.
- 71 O. García-Beltrán, B. K. Cassels, C. Pérez, N. Mena, M. T. Núñez, N. P. Martínez, P. Pavez and M. E. Aliaga, *Sensors*, 2014, **14**, 1358–1371.
- 72 R. Patil, A. Moirangthem, R. Butcher, N. Singh, A. Basu, K. Tayade, U. Fegade, D. Hundiwale and A. Kuwar, *Dalton Trans.*, 2014, **43**, 2895–2899.

